Journal of Power Sources 242 (2013) 57–64

Contents lists available at SciVerse ScienceDirect

Journal of Power Sources

journal homepage: www.elsevier.com/locate/jpowsour

Carbon–CeO_2 composite nanofibers as a promising support for a PtRu anode catalyst in a direct methanol fuel cell

Chen Feng, Taizo Takeuchi, Mohammad Ali Abdelkareem, Takuya Tsujiguchi, Nobuyoshi Nakagawa*

Department of Chemical and Environmental Engineering, Graduate School of Engineering, Gunma University, 1-5-1 Tenjin-cho, Kiryu, Gunma 376-8515, Japan

HIGHLIGHTS

- Carbon–CeO_2 composite nanofibers, (C-CeO_2)NF, have been electrospun.
- PtRu supported on (C-CeO_2)NF was proposed for the methanol electro-oxidation.
- Activity of the catalyst layer was evaluated on a glassy carbon electrode.
- Microstructure of the catalyst layer depended on catalyst and Nafion loadings.
- PtRu/(C–CeO_2)NF showed higher catalyst performance than commercial PtRu/C.

ARTICLE INFO

Article history:
Received 26 November 2012
Received in revised form
27 April 2013
Accepted 30 April 2013
Available online 23 May 2013

Keywords:
Carbon–CeO_2 composite nanofiber
Direct methanol fuel cells (DMFC)
Methanol oxidation reaction
Nafion content
Catalyst loading
Glassy carbon electrode (GCE)

ABSTRACT

Carbon–CeO_2 composite nanofibers, (C–CeO_2)NF, in which the CeO_2 nanoparticles were embedded in the carbon nanofibers, have been fabricated by electrospinning and used as a support for PtRu nanoparticles as the catalyst for methanol oxidation. The parameters affecting the performance of the catalyst layer structure on a glassy carbon electrode (GCE), such as the catalyst loading and the Nafion content in the catalyst layer, have been investigated. The catalyst layer prepared on the GCE with the nanofiber catalyst showed a different activity from that of the nanoparticle catalyst depending on both the loading of the catalyst and the Nafion content. There was an optimum Nafion content, 20 wt%, in the catalyst layer on the GCE for producing a homogenous layer structure. The homogenous layer structure with the nanofiber was obtained at a relatively high catalyst loading between 0.5 and 1.5 mg cm^{-2}. Under the optimum conditions, the catalyst layer with PtRu/(C–CeO_2)NF showed a significantly three times higher mass activity for the methanol oxidation and durability than that of the commercial PtRu/C catalyst due to the incorporation of the CeO_2 into the catalyst layer.

1. Introduction

Direct methanol fuel cells (DMFCs) have been intensively investigated due to their many advantages including high energy density, ease of handling, and low operating temperature [1–3]. One of the main obstacles facing the development of the DMFC is the low catalytic activity especially at the anode. The intermediate products, such as CO, from the methanol oxidation over the Pt surface are strongly adsorbed on the Pt surface and caused catalyst poisoning [4,5]. Pt is typically alloyed with Ru [6–9] to decrease the poisoning by providing OH species to facilitate the CO oxidation and removal from the Pt surface and participates in the methanol oxidation [6,7]. Although the Ru alloying improves the activity for the methanol oxidation reaction (MOR), it is still low.

The selection of a support for the Pt nanostructures is of key importance to both the catalytic activity and durability [10]. Various combinations with different supports have been developed, among which the utilization of transition metal oxide supports, such as CeO_2 [11–14], TiO_2 [15,16], SnO_2 [17,18], and WO_3 [19,20], has been reported. Particularly, CeO_2 has received considerable attention because it is a fluorite oxide whose cations can switch between the +3 and +4 oxidation states and therefore acts as an oxygen buffer. In addition, ceria enhances the catalytic performance by increasing the active metal dispersion on the support surface [21]. CeO_2 is normally used as a co-catalyst in fuel cell applications with different structures [21–26]. Whether Pt is deposited on the CeO_2 then followed by deposition on the carbon support [21] or CeO_2 is deposited on the carbon support followed by the deposition of the Pt thereon [22], the

* Corresponding author. Tel.: +81 277 30 1458; fax: +81 277 30 1457.
E-mail addresses: nakagawa@cee.gunma-u.ac.jp, nobnaka@sannet.ne.jp (N. Nakagawa).

0378-7753/$ – see front matter © 2013 Elsevier B.V. All rights reserved.
http://dx.doi.org/10.1016/j.jpowsour.2013.04.157

direct contact between the Pt and carbon was interrupted by the CeO_2. The direct mixture of the as-prepared catalyst, Pt/C, with CeO_2 nanoparticles was proposed as an easy way to avoid this problem [25,26]. The application of the CeO_2, of which the electrical conductivity is quite low compared to that of the carbon at the low operating temperatures, as a part of the catalyst layer in the MEA structure, requires a high electrical conduction through the layer to maximize the power output. The close and tight connection between the CeO_2 and carbon particles could enhance the electrical conductivity of the catalyst. The embedding of CeO_2 nanoparticles in the carbon nanofibers will be an ideal solution for providing a tight connection between the CeO_2 nanoparticles and the carbon.

Generally, for evaluation of the catalytic activity, a glassy carbon electrode (GCE) has been widely used as an easy and convenient way for the evaluation and comparison with the different catalysts, although the evaluation conditions of the catalyst on the surface of the glassy carbon may be different from that of the actual catalyst layer in the MEA structure. A small amount of catalyst is dispersed on the mirrored surface of the GCE, and its catalytic performance is evaluated in a three-electrode system by cyclic voltammetry, CV, and/or other measurement techniques. The activity would be strongly affected by the size and shape of the catalyst itself relating to the morphology of the catalyst layer on the GCE. A different shape of the catalyst, i.e., nanofiber or nanoparticle, would provide a different microstructure for the catalyst layer where the density of active sites of the catalyst and the mass transport resistance are different. The monomer content in the catalyst layer is also another parameter affecting the catalytic activity of the layer. The optimum content of the ionomer would be different for the different catalyst shapes. For a nanoparticle catalyst, there are some reports about the parameters affecting the performance of the catalyst layer such as the Nafion content, preparation method and catalyst loading [27–29]. Watanabe et al. investigated the effect of the Pt catalyst loading on the surface of a glassy carbon electrode on the ORR activity. They found that there is a linear dependence of the ORR activity on the Pt catalyst loading [27]. In another study, Nafion negatively affected the ORR activity where it blocks the sites available for O_2 adsorption on the Pt [28]. The application of a nanofiber structure for the catalyst or catalyst support in fuel cell catalyst applications is quite new and has significantly increased in the last few years. The parameters affecting the structure of the nanofiber catalyst layer on the glassy carbon electrode are more than those for the nanoparticles. For example, the aspect ratio of the catalyst is related to the orientation of the nanofibers in the layer and then to the porosity of the layer. Almost no reports have been conducted on the evaluation and optimization of the nanofiber catalyst layer structure on the glassy carbon electrode. In a comparison of the mass activity of the different catalysts using a GCE electrode, a linear dependence of the activity on the mass of the catalyst must be presumed. However, most of the previous reports on the nanofiber catalysts did not pay attention to this point.

In this study, a carbon–CeO_2 composite nanofiber, (C–CeO_2)NF, in which the CeO_2 nanoparticles were embedded into the carbon nanofiber, CNF, was prepared by an electrospinning technique and used as the support for the PtRu nanoparticle catalyst for the MOR. The catalytic activity of the prepared catalyst, PtRu/(C–CeO_2)NF, was evaluated by using a GCE and optimizing the preparation of the catalyst layer on it, i.e., the effect of ionomer content and the loading of the catalyst on the GCE. Using the optimum conditions for the nanofiber catalyst layer, the MOR activity of PtRu/(C–CeO_2)NF was compared to that of PtRu/CNF and a commercial nanoparticle catalyst. The results are discussed based on the effect of the CeO_2 embedding of the CNF support, and also based on the catalyst dispersion and morphology on the glassy carbon electrode investigated by an SEM examination.

2. Experimental

2.1. Preparation of the C–CeO_2 nanofiber support

Polyacrylonitrile (PAN, Sigma–Aldrich, Co., Ltd.) was used as the carbon source of the nanofiber. A PAN solution was prepared by dissolving it in dimethylformamide (DMF, Wako Pure Chemicals Ind., Ltd.) by stirring the mixture at 60 °C for 1 h. Ammonium cerium nitrate ($Ce(NH_4)_2(NO_3)_6$, Wako Co., Ltd.), as a the CeO_2 source, was dissolved in DMF and mixed with the PAN solution in the weight ratio of PAN to CeO_2 of 15 to 1. Another PAN solution without adding the CeO_2 source was also prepared for the CNF support as a reference. The mixture was further mixed for another 1 h and then transferred to a glass syringe attached to a stainless steel needle for the electrospinning.

Electrospinning [30] of the precursor mixture was conducted by applying 17 kV between the needle and a metallic collector covered with aluminum foil at a distance of 12 cm between them, and feeding the solution at 0.05 ml min^{-1} into the electric field. A high voltage power supply (Pulse Electronic Engineering Co., Ltd.) with the maximum voltage of 50 kV was used to apply the high voltage, and a syringe pump (Future Science Co., Ltd.) was used to control the solution flow rate. The nanofiber mats formed on the collector were initially dried in air for 3 h at room temperature and then stabilized by heating at 240 °C in air for 3 h. The stabilized nanofibers were carbonized in a nitrogen atmosphere at 900 °C, which was selected as the optimum temperature for good carbonization and a small CeO_2 grain size, for 1 h. The heating rate was fixed at 5 °C min^{-1}. The obtained nanofibers were then milled using an agate mortar for 30 min to normalize the fiber length.

2.2. PtRu nanoparticle deposition

PtRu nanoparticles were deposited on the cerium oxide-carbon nanofiber (C–CeO_2)NF and on the CNF without CeO_2. The support material was ultrasonically dispersed in a mixture of distilled water and isopropyl alcohol for 20 min. 20 wt% Pt–Ru (in an atomic ratio of 1:1) was obtained by the chemical reduction of H_2PtCl_6 and $RuCl_3$ as precursors at 80 °C using sodium borohydride. The pH value of the ink was adjusted with a NaOH solution to 8 and then its temperature was raised to 80 °C. Twenty-five milliliters of 0.2 M solution of sodium borohydride was dropwise added to the ink with stirring for 1 h. The mixture was cooled, dried and repeatedly washed with distilled water. The catalyst was dried for 3 h at 120 °C.

2.3. Characterization of the catalyst

The surface morphology and elemental analysis of the prepared catalyst were studied by FE-SEM equipped with EDX (Hitachi S-7400, Hitachi Co., Ltd.). A high-resolution image of a selected area was observed by a JEOL JEM 2010 transmission electron microscope (TEM) operating at 200 kV. The crystal structure of the prepared PtRu catalyst was investigated based on the X-ray diffraction (XRD) patterns of the powder samples using an X-ray diffractometer (RINT2100/PC, Rigaku Corp.). The X-ray source was Cu-Kα, operating at 32 kV and 20 mA. The crystalline sizes, d, of the PtRu and CeO_2 were calculated by the width of the peak at half-height for the Pt(111) at 40° and CeO_2(111) at 28.5° using Scherrer's equation.

$$d = 0.9\lambda/\beta \cos\theta$$

where λ is the wavelength of the X-ray (1.54056 Å), θ is the angle at the peak, and β is the width of the peak at half-height.

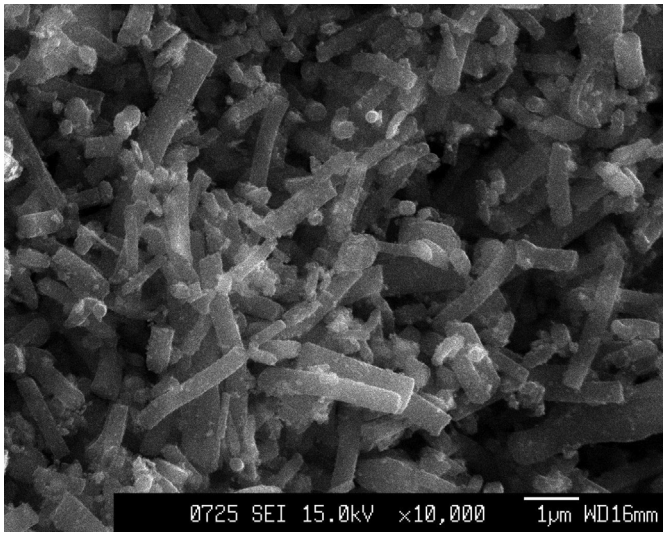

Fig. 1. FE-SEM image of the PtRu/(C–CeO_2)NF.

2.4. Electrochemical measurements

The MOR activity of the prepared catalyst was investigated by cyclic voltammetry in a three-electrode cell with a fixed glassy carbon electrode (GCE) (3-mm diameter) at room temperature. The catalyst ink was prepared by dispersing a certain amount of the catalyst in a water, ethanol and 5 wt% Nafion solution, then the mixture was ultrasonicated for 30 min. A thin film of the catalyst on the GCE was prepared by depositing 2.5 μL of the catalyst ink on the glassy carbon electrode. The electrode was dried at room temperature in air for 1 h, then heated in an oven at 90 °C for 30 min. As a reference, the PtRu nanoparticles deposited on a carbon black support, a commercial PtRu/C, Tanaka Kikinzoku, PtRu (53.3 wt%), was used, and its MOR activity was measured in a similar manner. The results were then compared to those of the prepared nanofiber catalysts.

The effect of the Nafion content in the catalyst ink, i.e., the Nafion [g]/catalyst [g], on the performance was investigated while maintaining a catalyst loading of 0.5 mg cm^{-2}. The effect of the catalyst loading on the performance was investigated by changing the amount of the catalyst in the ink to yield a different final catalyst loading on the glassy carbon electrode from 0.21 to 1.53 mg cm^{-2} while maintaining a constant Nafion content in the catalyst at 20 wt%.

A Pt wire and an Ag/AgCl/KCl electrode were used as the counter and reference electrodes, respectively. The electrolyte was a solution of 2 M methanol in 0.5 M H_2SO_4. Nitrogen was bubbled into the solution for 20 min to maintain an oxygen-free atmosphere near the working electrode.

The activity of the prepared catalyst was expressed based on the apparent electrode area of the glassy carbon electrode except for the case specifically mentioned. The MOR activity was investigated by CV in the potential range from −0.2 to 1.4 or 1.6 V vs. NHE at the scan rate of 20 mV s^{-2} with N_2 bubbling at room temperature and by chronoamperometry, CA, at 0.8 V vs. NHE for 60 min. The measurements were conducted using an electrochemical measurement system (HAG-5010, Hokuto Denko Co., Ltd.).

3. Results and discussion

3.1. Analysis of the prepared catalyst

Fig. 1 shows the FE-SEM image of the prepared PtRu catalyst on a (C–CeO_2)NF support, PtRu/(C–CeO_2)NF. The nanofiber support had a diameter of 300–400 nm and a length of less than 2 μm. The small dots of about 10 nm in diameter over the nanofibers were the PtRu nanoparticles, because these particles were not detected on the support before the PtRu deposition, although the images of the support before the catalyst deposition are not shown.

Fig. 2 shows the TEM images of the prepared PtRu/(C–CeO_2)NF at different resolutions, i.e., a low resolution, Fig. 2(a), and a high resolution, Fig. 2(b). The nanofiber morphology was clear in the image and the small particles dispersed on the support nanofiber would be the PtRu nanoparticles, Fig. 2(a). The big particles of around 15 nm in diameter in the nanofibers were the CeO_2 nanoparticles as confirmed by measuring the interplanar spacing of 0.32 nm that is in agreement with the CeO_2 (111) facet distance, Fig. 2(b). The interplanar spacing of the PtRu particles is not clear in this figure.

Fig. 3 shows the XRD pattern of the PtRu/(C–CeO_2)NF and that of the (C–CeO_2) NF support. The PtRu alloy catalysts showed a face-centered cubic structure; a slight shift in the peak position for Pt(111), 40.0, from that of pure platinum, 39.8, is related to the Ru alloying effect [9]. CeO_2 also showed a face-centered cubic structure at different peak positions as shown in the figure. The positions of the CeO_2 peaks were not affected by the catalyst preparation as shown in the figure.

Table 1 summarizes the elemental analysis and crystalline size of the PtRu catalyst measured by EDX and XRD, respectively. The calculated crystalline size of the PtRu on the (C–CeO_2) NF, based on the XRD analysis, was 9.9 nm, which is slightly larger than that of the commercial PtRu catalyst, PtRu/C_{com}, of 7.7 nm. CeO_2 had a crystal size of 16.5 nm that is in accordance with that in the TEM images, Fig. 2(b). The elemental analysis by EDX showed that PtRu in the atomic ratio 1 to 1 was successfully prepared with the desired loading of 20 wt% for the PtRu.

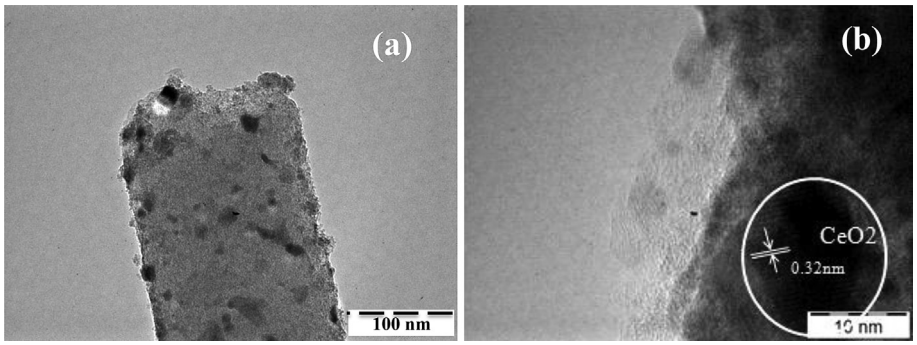

Fig. 2. TEM images of the prepared PtRu/(C–CeO_2)NF at (a) low magnification and (b) high magnification.

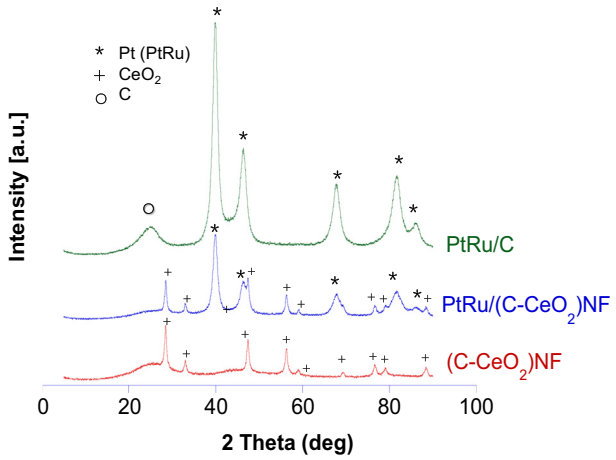

Fig. 3. XRD patterns of the prepared (C–CeO_2)NF and PtRu/(C–CeO_2)NF as well as that of PtRu/C_{com}.

3.2. Effect of Nafion content and catalyst loading on the GCE

Fig. 4 shows the effect of the Nafion content in the catalyst layer on the CV curves for the MOR of (a) PtRu/(C–CeO_2)NF, (b) PtRu/C_{com}, and (c) PtRu/CNF. The catalyst loading in these experiments was maintained at 0.5 mg cm^{-2}. For the PtRu/(C–CeO_2)NF, the oxidation peak current density at around 1 V vs. NHE increased with the increasing Nafion-to-catalyst ratio from 15 mA cm^{-2} at the ratio of 0.025–55 mA cm^{-2} at 0.2, then decreased with a further increase in the Nafion-to-catalyst ratio. Similarly, the peak current density for PtRu/CNF became a maximum at the ratio of 0.2 although the magnitude of the peak current density was lower than that of PtRu/(C–CeO_2)NF. On the other hand, for the PtRu/C_{com}, the peak current density was slightly affected by the change in the Nafion-to-catalyst ratio in the measured ratio range of 0.025 to 1.5. Fig. 5 shows the effect of the Nafion-to-catalyst ratio on the oxidation peak current density. The change in the Nafion content has almost no effect on the MOR activity of the nanoparticle catalyst, PtRu/C_{com}, while there was an optimum Nafion content, a Nafion-to-catalyst ratio of 0.2 to 0.5, for the nanofiber catalyst structures, PtRu/(C–CeO_2) NF and PtRu/CNF.

Fig. 6 shows the surface morphology of the PtRu/(C–CeO_2)NF catalyst layer on the glassy carbon electrode using different Nafion-to-catalyst ratios, (a) 0.025, (b) 0.2 (c) 0.5 and (d) 1.5. At the lowest Nafion-to-catalyst ratio, 0.025, segregation of the catalyst significantly occurred on the GCE surface and the catalyst did not cover the entire surface. Therefore, the catalyst was not efficiently used and thus showed a low performance. With the increase in the Nafion-to-catalyst ratio to 0.2 and 0.5, the catalyst dispersion over the electrode was significantly improved and a homogenous catalyst layer formed and covered the entire electrode surface, Fig. 6(b) and (c); therefore, the performance increased. A further increase in the Nafion-to-catalyst ratio to 1.5 resulted in bundling the catalyst nanofibers together by the excess Nafion to form the catalyst layer, Fig. 6(d); therefore, the performance decreased.

As is clear in Fig. 6(a), there was a big variation in the length of the nanofiber up to tens of nanometers. At the low Nafion-to-catalyst ratio, 0.025, poor bridging occurred between these nanofibers over the entire surface of the GCE, Fig. 6(a), i.e., the Nafion content was too low to bridge the catalyst nanofibers together. With an increase in the Nafion content, Nafion could form bridges between the different nanofiber lengths and homogeneously cover the entire GCE surface, Fig. 6(b) and (c); therefore, a better catalyst distribution was obtained. At a higher Nafion content, the excess Nafion controlled the homogenous bridging of the nanofibers in the layer by forming bundles of the nanofibers with the Nafion in the layer, therefore, limiting the catalyst active sites in the layer.

Fig. 7 shows the effect of the catalyst loading on the GCE on the MOR activity of (a) PtRu/(C–CeO_2)NF, (b) PtRu/C_{com} and (c) PtRu/CNF catalyst. The oxidation peak current density at around 1 V vs. NHE increased with the increase in the catalyst loading among the different catalysts. Fig. 8(a) shows the effect of the catalyst loading on the MOR peak potential. With an increase in the catalyst loading, there was a shift in the MOR peak potential to a higher value especially at the high current densities. The shift in the MOR peak potential with the increase in the catalyst loading can be explained by the increase in the IR drop through the thickness of the catalyst layer formed on the GCE at the different catalyst loadings. The increase in the catalyst loading resulted in an increase in the thickness of the catalyst layer, therefore, the IR drop through the catalyst layer thickness increased, and thus, a shift in the peak potential appeared. Fig. 8(b) shows the effect of the catalyst loading on the MOR peak current density. The peak current density increased with the increase in the catalyst loading. At low catalyst loading of 0.25 mg cm^{-2} (−0.6 on the *x* axis), the PtRu supported on the nanofiber structure showed a lower performance than the particle catalyst, PtRu/C_{com}. With the increase in the catalyst loading to 0.5 mg cm^{-2} (−0.3 on the *x* axis), the performances of the different catalysts were similar, while at the higher catalyst loading, the PtRu/(C–CeO_2)NF catalyst showed a higher performance than the particle catalyst, PtRu/C_{com}. To clarify the reason for the difference in the activity between the two catalysts, i.e., nanoparticle and nanofiber, the surface morphologies of the different catalyst layers at the different loadings on the glassy carbon electrode were investigated. Fig. 9 shows the surface morphology of the PtRu/(C–CeO_2)NF catalyst layer using different catalyst loadings, (a) 0.25 mg cm^{-2}, (b) 0.45 mg cm^{-2} and (c) 1.08 mg cm^{-2}. At the low catalyst loading, Fig. 9(a), the somewhat heterogenous catalyst layer on the entire surface of the electrode was formed, therefore, the electrode was not efficiently used. With the increase in the catalyst loading, the entire surface of the electrode was homogeneously covered with the nanofiber catalyst, Fig. 9(b) and (c). The low performance in the case of the nanofiber structure at a low catalyst loading would be related to the heterogenous dispersion of the catalyst on the GCE surface, i.e., the loading of 0.25 mg cm^{-2} was too low to form a homogenous layer of the catalyst over the entire surface of the electrode. On the other hand, in the case of the nanoparticle catalyst, the catalyst loading of 0.25 mg cm^{-2} was sufficient to form a complete homogenous layer of the catalyst over the entire electrode surface as shown in Fig. 10(a). Although at a

Table 1
Properties of the PtRu catalyst with the different supports measured with XRD and EDX.

Catalyst	Composition [wt%]					Pt/Ru [atm/atm]	PtRu loading [wt%]	PtRu crystalline size [nm]	CeO_2 crystalline size [nm]
	Pt	Ru	C	Ce	O				
PtRu/C_{com}	30.0	23.3	46.7	–	–	1.29	53.3	7.7	–
PtRu/CNF	13.4	6.9	70.4	–	9.3	1.01	20.3	5.0	–
PtRu/(C–CeO_2)NF	13.9	6.3	55.9	17.3	6.6	1.14	20.2	9.9	16.5

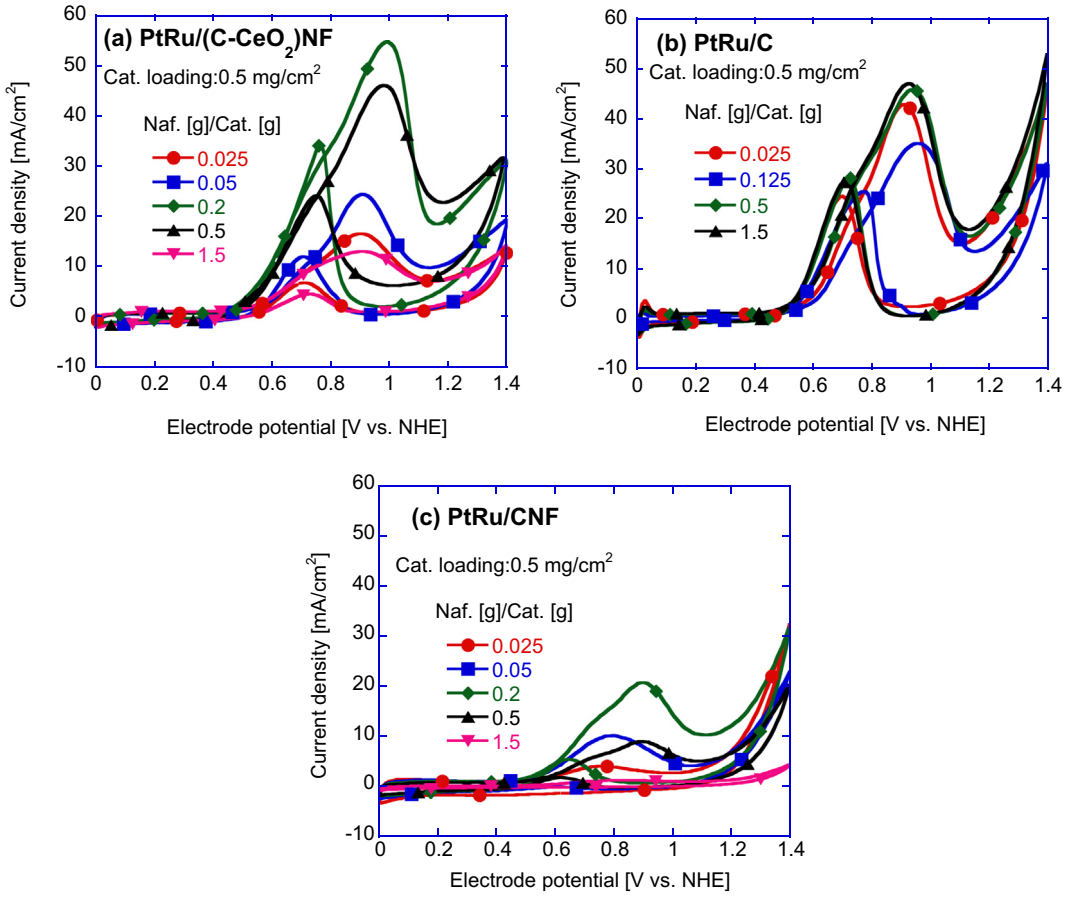

Fig. 4. Effect of Nafion content in the catalyst layer (Nafion [g]/catalyst [g]) on the performance of the catalyst at the catalyst loading of 0.5 mg cm^{-2}: (a) PtRu/(C–CeO_2)NF, (b) PtRu/C_{com} and (c) PtRu/CNF.

high catalyst loading over 1 mg cm^{-2}, both the nanofiber and nanoparticle catalysts showed a linear dependence of the performance on the catalyst loading, Fig. 8(b), the nanofiber catalyst, PtRu/(C–CeO_2)NF, showed the best performance and this would be related to the higher porosities in the nanofiber catalyst layer, Fig. 9(c), than that in the case of the nanoparticle structure, Fig. 10(b).

When the actual application of the catalyst in the MEA structure requires high a catalyst loading usually over 1 mg cm^{-2}, the nanofiber structure was expected to provide a better performance under an actual application in fuel cells. This is now under investigation.

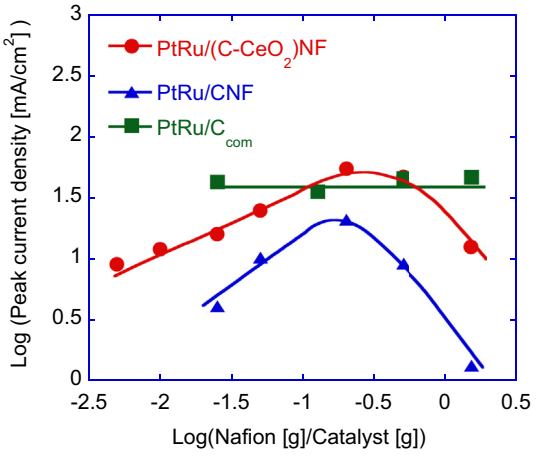

Fig. 5. Effect of Nafion content in the catalyst layer (Nafion [g]/catalyst [g]) on the peak current density of the different catalysts.

3.3. Comparison among the PtRu/(C–CeO_2)NF, PtRu/CNF and commercial catalyst

The activity of the nanofiber catalyst layer depended on the ionomer content in the catalyst layer and the catalyst loading on the GCE as shown in Figs. 5 and 8(b), respectively. The target of the evaluation of the prepared catalyst is their application as a catalyst layer in the DMFC. A high catalyst loading of over 1 mg cm^{-2} is usually required, and this loading was in the region in which the nanofiber catalyst showed a linear dependence of the activity on the catalyst loading with a homogenous layer structure. Based on there results, a comparison of the catalytic activity between the nanofiber catalysts and the nanoparticle catalysts was conducted under the optimum conditions for the nanofiber catalyst, i.e., the Nafion/catalyst ratio was 0.2 and the catalyst loading was 1.24 mg cm^{-2} at which the linear dependence of the activity on the loading was confirmed for both the nanofiber catalyst and the particle catalyst as shown in Fig. 8(b).

Fig. 11 shows the comparison of the MOR activity among the PtRu/(C–CeO_2)NF, PtRu/CNF and PtRu/C_{com} catalysts based on mg-PtRu. The PtRu supported on the (C–CeO_2)NF showed the best MOR activity, i.e., a higher peak current density than that of the commercial catalyst. The peak current density appeared at 1.2 V vs. NHE for the PtRu/(C–CeO_2) NF vs. 1.05 V vs. NHE for the PtRu/CNF and the commercial catalyst. The higher peak potential for the PtRu/(C–

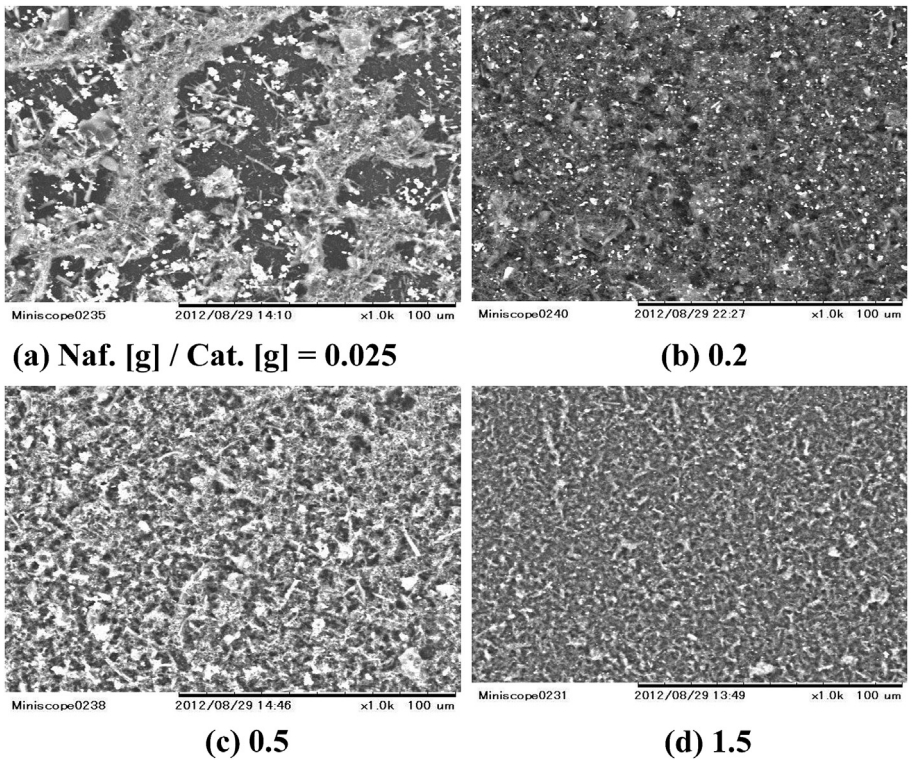

Fig. 6. Surface morphology of the PtRu/(C–CeO_2)NF catalyst layer over the GCE using different Nafion [g]/catalyst [g] ratios: (a) 0.025, (b) 0.2, (c) 0.5 and (d) 1.5.

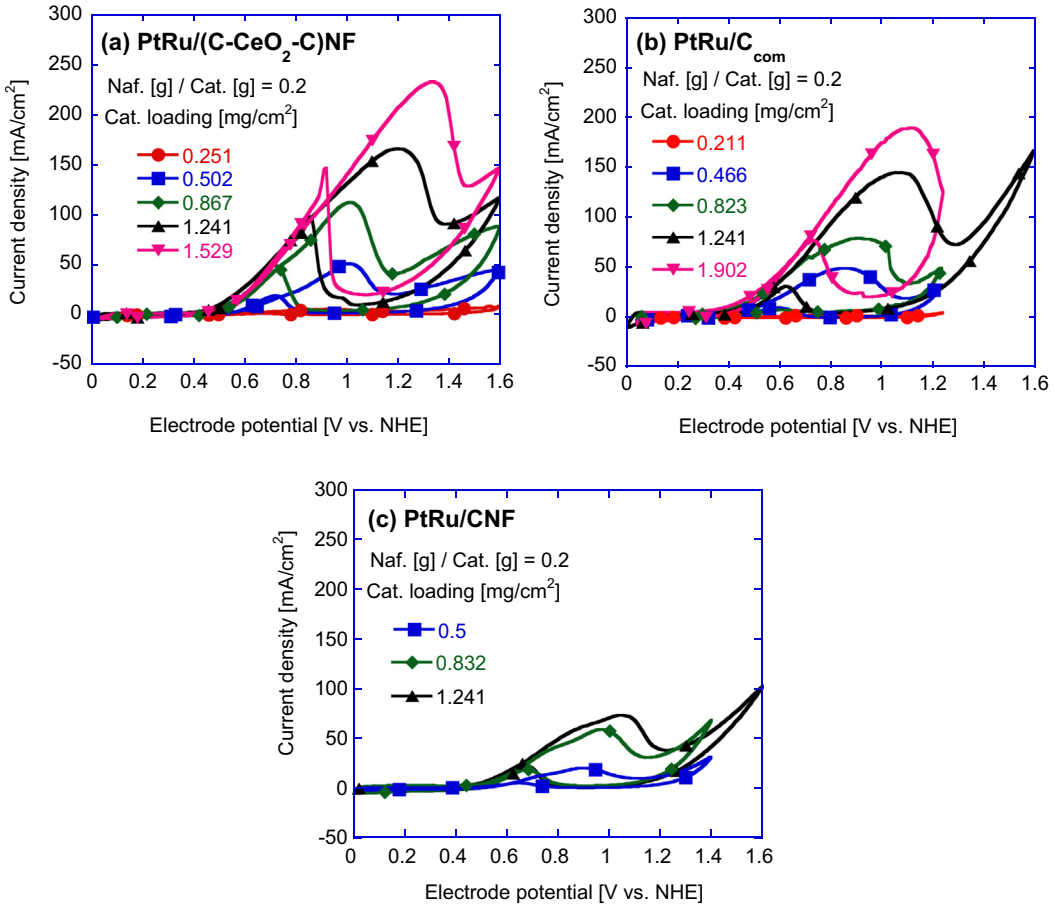

Fig. 7. The effect of catalyst loading on the GCE surface on the CV performance when Naf. [g]/cat. [g] was 0.2 : (a) PtRu/(C–CeO_2) NF, (b) PtRu/C_{com} and (c) PtRu/CNF.

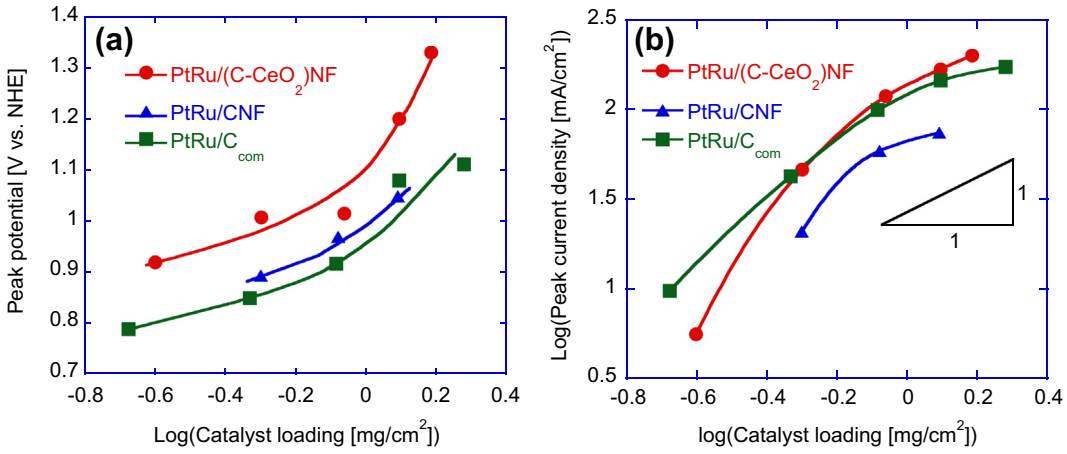

Fig. 8. Effect of catalyst loading of the different catalysts on the surface of the GCE on: (a) MOR peak potential, (b) peak current density.

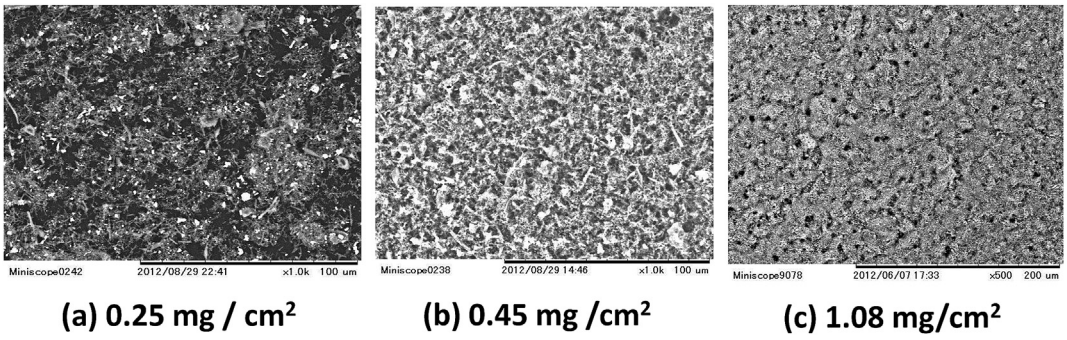

Fig. 9. Surface morphology of the PtRu/(C–CeO_2)NF catalyst layer on the GCE using different catalyst loadings: (a) 0.25, (b) 0.45 and (c) 1.08 mg cm^{-2}.

CeO_2)NF would mainly due to the higher IR resistance through the catalyst layer. The higher IR resistance of the layer for PtRu/(C–CeO_2)NF compared to that of PtRu/CNF is reasonable because the former nanofiber contained low electro-conductive particles, CeO_2, in it. The peak current density, i.e., mass activity, for the PtRu/(C–CeO_2)NF was around 680 mA $(mg_{\text{-PtRu}})^{-1}$, which was more than two times higher than that of the PtRu/CNF, 280 mA $(mg_{\text{-PtRu}})^{-1}$, and three times higher than that of the commercial catalyst, 200 mA $(mg_{\text{-PtRu}})^{-1}$. One may request the comparison in the mass activity between the PtRu/CNF and PtRu/C at the same PtRu loading, 20 wt %, while the loading for the commercial catalyst was as high as 55 wt%, since the mass activity generally decreases with the increase of the metal loading on the support [31]. We have already compared the mass activity of the PtRu/CNF and that of PtRu/C (C, Vulcan XC-72) of which PtRu crystalline size (9.4 nm), Pt/Ru atomic ratio (0.93) and PtRu loading (16 wt%) were similar to that of the PtRu/CNF. The results showed a 1.6 times higher mass activity for the PtRu/CNF than that of the PtRu/C [32]. By including this additional information, the mass activity was high in the order of PtRu/(C–CeO_2)NF > PtRu/CNF > PtRu/C_{com} (>PtRu/C). The significant positive effect of CeO_2 embedded on the carbon nanofiber support on the catalytic activity was confirmed in the figure. In previous reports, the direct mixture of CeO_2 nanoparticles with the commercial catalysts Pt/C [25] and PtRu/C [26] enhanced the MOR mass activity by 1.3 and 1.6 times, respectively. The deposition of CeO_2 over the carbon nanoparticle [21] or carbon nanotube [24] support followed by Pt deposition enhanced the MOR mass activity by 1.6 times in both cases. These previous reports showed an increase in

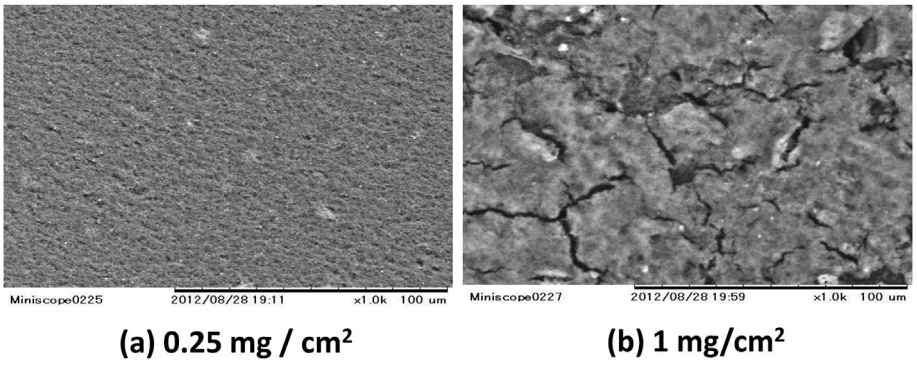

Fig. 10. Surface morphology of the PtRu/C_{com} catalyst layer on the GCE using different catalyst loadings: (a) 0.25 and (b) 1 mg cm^{-2}.

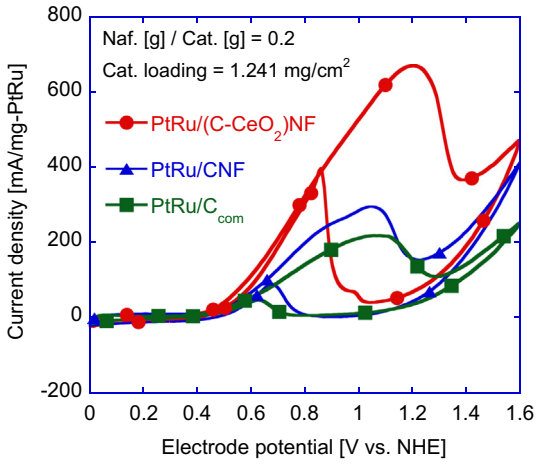

Fig. 11. MOR activity of the PtRu/(C–CeO_2)NF, PtRu/CNF and PtRu/C_{com} catalysts at the optimum preparation conditions for the catalyst layer on the GCE.

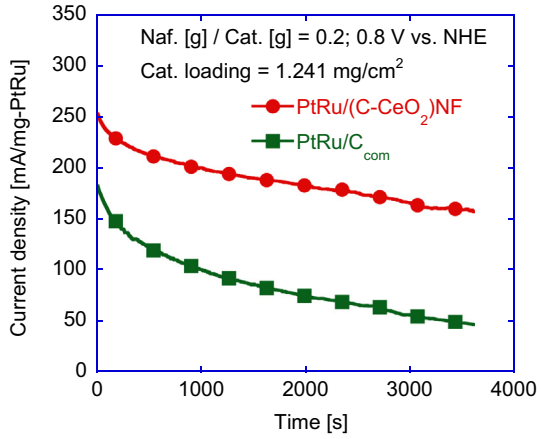

Fig. 12. CA measurement of the PtRu/(C–CeO_2)NF catalyst and PtRu/C_{com} catalysts at 0.8 V vs. NHE.

the MOR activity by employing CeO_2 nanoparticles not more than 2 times, and the change was not as high as that found in this study.

Fig. 12 shows the CA profiles measured for the PtRu/(C–CeO_2)NF catalyst and that for the commercial catalyst at 0.8 V vs. NHE. The initial current density was higher for the PtRu/(C–CeO_2)NF than that of the commercial catalyst. The current decreased in both of the two cases but at a lower rate for the PtRu/(C–CeO_2)NF. After 1 h of operation, the PtRu/(C–CeO_2)NF lost 37.8% of the initial performance compared to a 74.4% loss for the commercial catalyst, and the steady current density after 1 h of operation was three times higher than that of the commercial catalyst thus showing the higher MOR activity with the higher stability.

Such a high MOR activity and stability of the PtRu/(C–CeO_2)NF would be explained by the intimate contact between the CeO_2 nanoparticles and the carbon achieved by embedding the CeO_2 particles in the CNF. This nanostructure promoted the electron conduction between them, then the consecutive reaction process of the methanol oxidation on the surface of the catalyst, was enhanced by the CeO_2.

4. Conclusions

Carbon–CeO_2 composite nanofibers, in which the CeO_2 nanoparticles are embedded in the carbon nanofiber, have been fabricated by electrospinning and used as a support for the PtRu nanoparticles as the catalyst for methanol oxidation. The parameters affecting the performance of the layer structure on a GCE have been investigated and the following conclusions were drawn: The catalyst layer prepared on the GCE with the nanofiber catalyst showed a different activity depending on both the loading of the catalyst and the Nafion content that affected the morphology of the catalyst layer on the electrode surface. The nanofiber structure at a high catalyst loading over 0.5 mg cm^{-2}, which is recommended for the actual fuel cell application, is better than that of the nanoparticles due to the homogenous layer structure. The catalyst layer with PtRu/(C–CeO_2) NF showed a significantly greater activity and stability compared to that of the catalyst layer using a commercial PtRu/C catalyst. This was due to the incorporation of the CeO_2 in the catalyst layer.

Acknowledgments

Part of this work was supported by the Element Innovation Project, Ministry of Education, Japan. Mohammad Ali Abdelkareem thanks JSPS for a fellowship.

References

[1] A.S. Aricò, S. Srinivasan, V. Antonucci, Fuel Cells 1 (2001) 133–161.
[2] T. Tsujiguchi, M.A. Abdelkareem, T. Kudo, N. Nakagawa, T. Shimizu, M. Matsuda, J. Power Sources 195 (2010) 5975–5979.
[3] N. Nakagawa, T. Tsujiguchi, S. Sakurai, R. Aoki, J. Power Sources 192 (2012) 325–332.
[4] A. Hamnett, Catalyst Today 38 (1997) 445–457.
[5] R. Manoharan, J.B. Goodenough, J. Mater. Chem. 2 (1992) 875–887.
[6] M. Watanabe, S. Motoo, J. Electroanal. Chem. 60 (1975) 267–273.
[7] K.A. Friedrich, K.P. Geyzers, U. Linke, U. Stimming, J. Stumper, J. Electroanal. Chem. 402 (1996) 123–128.
[8] J.W. Guo, T.S. Zhao, J. Prabhuram, R. Chen, C.W. Wong, Electrochim. Acta 51 (2005) 754–763.
[9] M.-S. Loffler, H. Natter, R. Hempelmann, K. Wippermann, Electrochim. Acta 48 (2003) 3047–3051.
[10] S. Sharma, B.G. Pollet, J. Power Sources 208 (2012) 96–119.
[11] C.L. Campos, C. Roldan, M. Aponte, Y. Ishikawa, C.R. Cabrera, J. Electroanal. Chem. 581 (2005) 206–215.
[12] D.-M. Gu, Y.-Y. Chu, Z.-B. Wang, Z.-Z. Jiang, G.-P. Yin, Y. Liu, Appl. Catal. B 102 (2011) 9–18.
[13] A.O. Neto, L.A. Farias, R.R. Dias, M. Brandalise, M. Linardi, E.V. Spinace, Electrochem. Commun. 10 (2008) 1315–1317.
[14] S. Supakanapitak, V. Boonamnuayvitaya, S. Jarudilokkul, J. Chem. Eng. Jpn. 45 (2012) 544–550.
[15] K. Drew, G. Girishkumar, K. Vinodgopal, P.V. Kamat, J. Phys. Chem. B 109 (2005) 11851–11857.
[16] S.-Y. Huang, P. Ganesan, S. Park, B.N. Popov, J. Am. Chem. Soc. 131 (2009) 13898–13899.
[17] X.W. Lou, D. Deng, J.Y. Lee, L.A. Archer, Chem. Mater. 20 (2008) 6562.
[18] H.L. Pang, X.H. Zhang, X.X. Zhong, B. Liu, X.G. Wei, Y.F. Kuang, J.H. Chen, J. Colloid Interface Sci. 319 (2008) 193–198.
[19] S. Jayaraman, T.F. Jaramillo, S.-H. Baeck, E.W. McFarland, J. Phys. Chem. B 109 (2005) 22958–22966.
[20] Z. Cui, L. Feng, C. Liu, W. Xing, J. Power Sources 196 (2011) 2621–2626.
[21] M.A. Scibioh, S. Kim, E. Cho, T. Lim, S. Hong, H.Y. Ha, Appl. Catal. B Environ. 84 (2008) 773–782.
[22] M. Takahashi, T. Mori, F. Ye, A. Vinu, J. Am. Ceram. Soc. 90 (2007) 1291–1294.
[23] H.B. Yu, J. Kim, M.A. Scibioh, J. Lee, J. Han, S.P. Yoon, H. Yong Ha, J. Power Sources 140 (2005) 59–65.
[24] J. Wang, J. Xi, Y. Bai, Y. Shen, J. Sun, L. Chen, W. Zhu, X. Qiu, J. Power Sources 164 (2007) 555–560.
[25] L. Yu, J. Xi, Int. J. Hydrogen Energy 37 (2012) 15938–15947.
[26] J. Wang, X. Deng, J. Xi, L. Chen, W. Zhu, X. Qiu, J. Power Sources 170 (2007) 297–302.
[27] E. Higuchi, H. Uchida, M. Watanabe, J. Electroanal. Chem. 583 (2005) 69–76.
[28] A. Ohma, K. Fushinobu, K. Okazaki, Electrochim. Acta 55 (2010) 8829–8838.
[29] K. Ke, K. Hiroshima, Y. Kamitaka, T. Hatanaka, Y. Morimoto, Electrochim. Acta 72 (2012) 120–128.
[30] X. Sakai, K. Kawakami, M. Taya, J. Chem. Eng. Jpn. 45 (2012) 436–440.
[31] Y.-H. Cho, H.-S. Park, Y.-H. Cho, D.-S. Jung, H.-Y. Park, Y.-E. Sung, J. Power Sources 172 (2007) 89–93.
[32] Y. Ito, T. Takeuchi, T. Tsujiguchi, M.A. Abdelkareem, N. Nakagawa, J. Power Sources 242 (2013) 280–288.